Selective Facet Reactivity During Cation Exchange in Cadmium Sulfide Nanorods

Bryce Sadtler[1,2], Denis O. Demchenko[3], Haimei Zheng[1,2], Steven M. Hughes[1], Maxwell G. Merkle[1], Ulrich Dahmen[2], Lin-Wang Wang[3], A. Paul Alivisatos**[1,2]*

[1] Department of Chemistry, University of California, Berkeley, CA 94720

[2] Materials Science Division, Lawrence Berkeley National Laboratory, CA 94720,

[3] Computational Research Division, Lawrence Berkeley National Laboratory, Berkeley, CA 94720

AUTHOR EMAIL ADDRESS alivis@berkeley.edu

RECEIVED DATE (to be automatically inserted after your manuscript is accepted if required according to the journal that you are submitting your paper to)

CORRESPONDING AUTHOR FOOTNOTE

* Current address: Department of Physics, Virginia Commonwealth University, Richmond, VA 23284

** To whom correspondence should be addressed

ABSTRACT

The partial transformation of ionic nanocrystals through cation exchange has been used to synthesize nanocrystal heterostructures. We demonstrate that the selectivity for cation exchange to take place at different facets of the nanocrystal plays an important role in determining the resulting morphology of the binary heterostructure. In the case of copper I (Cu^+) cation exchange in cadmium

sulfide (CdS) nanorods, the reaction starts preferentially at the ends of the nanorods such that copper sulfide (Cu_2S) grows inwards from either end. The resulting morphology is very different from the striped pattern obtained in our previous studies of silver I (Ag^+) exchange in CdS nanorods where non-selective nucleation of silver sulfide (Ag_2S) occurs.[1] From interface formation energies calculated for several models of epitaxial connections between CdS and Cu_2S or Ag_2S, we infer the relative stability of each interface during the nucleation and growth of Cu_2S or Ag_2S within the CdS nanorods. The epitaxial connections of Cu_2S to the end facets of CdS nanorods minimize the formation energy, making these interfaces stable throughout the exchange reaction. However, as the two end facets of wurtzite CdS nanorods are crystallographically nonequivalent, asymmetric heterostructures can be produced.

INTRODUCTION

The synthesis of nanocrystal heterostructures, consisting of two or more components within each particle, is important both for creating multi-functional materials and for controlling electronic coupling between nanoscale units.[2-5] As the complexity of colloidal nanocrystal heterostructures increases beyond simple spherical core-shell morphologies, their electronic structure and physical properties will strongly depend on the spatial organization of the two materials within each nanocrystal. Colloidal nanocrystals possessing anisotropic shapes provide a platform for selective chemical modification based on the relative reactivities of the different crystalline facets exposed at the surface. This enables the synthesis of multi-component nanostructures through the nucleation and growth of a secondary material on specific facets of the nanocrystals.[4-11] While the methodology of sequential growth has been applied to a wide range of material combinations, its drawback is that the desired heterogeneous nucleation on the existing nanocrystal surface often competes with homogenous nucleation of separate nanocrystals of the secondary material.

An alternative method for synthesizing nanocrystal heterostructures, which circumvents separate nucleation, is the transformation of a portion of the nanocrystal into a new composition or structural phase.[12-17] In ionic nanocrystals, cation exchange reactions have been used to alter the composition of the material by replacing the cations within the nanocrystal lattice with a different metal ion.[1,15-20] For example, the addition of a small molar excess of Ag^+ cations to cadmium chalcogenide nanocrystals (CdS, CdSe, CdTe) leads to their complete conversion to the corresponding silver chalcogenide.[17] Remarkably, the shape of anisotropic nanocrystals such as rods and tetrapods is preserved after cation exchange when their dimensions are greater than the reaction zone for exchange (~ 4 nm), indicating that the cohesion of the crystal is maintained during the diffusion and exchange of cations. The relative rigidity of the anion sublattice enables the partial transformation of the nanocrystal to create a heterostructure where the two compounds share a common anion. Adjusting the ratio of substitutional cations to those within the nanocrystals can be used to control the relative volume fraction of the two crystals within the binary heterostructures.[1] The spatial arrangement of materials within the nanocrystal will depend on a number of kinetic and thermodynamic factors such as the relative activation barriers for cation exchange to initiate at different facets of the nanocrystal and the energetic stability of interfaces as reaction fronts proceed through the nanocrystal. In the case of Ag^+ exchange in CdS nanorods, the reorganization of Ag_2S and CdS regions via cation diffusion produces significant changes in the morphology of the heterostructures as the fraction of Ag_2S increases within each nanorod.[1,21] Low amounts of Ag^+ produce small Ag_2S regions dotting the surface of the nanocrystals, whereas greater amounts of Ag^+ lead to alternating segments of CdS and Ag_2S along the nanorod. The large lattice strain between CdS and Ag_2S is believed to play an important role in forming the striped pattern observed for this system. Thus, it is interesting to examine a case where the lattices of the cation exchange pair have little mismatch between them.

Here we report on the synthesis of CdS-Cu_2S nanorod heterostructures synthesized by partial Cu^+ exchange. The Cu_2S regions primarily occur at one or both ends of the nanorods and appear to

nucleate and grow along a single crystallographic direction. To elucidate why Cu^+ and Ag^+ cation exchange with CdS nanorods produce different morphologies, models for epitaxial connections between various facets of CdS with Cu_2S or Ag_2S lattices were used to calculate interface formation energies.[21] The formation energies indicate the favorability for interface nucleation at different facets of the nanorod and the stability of the interfaces during growth of the secondary material (Cu_2S or Ag_2S) within the CdS nanocrystal. Furthermore, the values of the interface formation energies provided by our models suggest that the asymmetric CdS-Cu_2S heterostructures observed are produced by selective Cu_2S nucleation on the $(000\bar{1})$ CdS end facet, as this interface has a lower formation energy than the attachment of Cu_2S to the opposite (0001) end.

EXPERIMENTAL

I. Synthesis of CdS nanorods. Colloidal CdS nanorods were synthesized using standard techniques developed for cadmium chalcogenide nanorods.[22] The reactions were performed under air-free conditions and the CdS nanocrystals were stored in an argon glove box. The Supporting Information provides specific reaction conditions and cleaning procedures for each batch of CdS nanorods used in this study.

II. Cation exchange of CdS nanorods. Cu^+ cation exchange was used to convert CdS nanorods into CdS-Cu_2S binary nanorods and Cu_2S nanorods. The reactions were performed inside an argon glove box at room temperature. The extent of conversion depends on the Cu^+/Cd^{2+} ratio, where an excess of Cu^+ ions ($Cu^+/Cd^{2+} > 2$ as two Cu^+ ions replace one Cd^{2+} ion for charge balance) leads to full conversion to Cu_2S. The molar concentration of Cd^{2+} ions for each CdS nanorod solution was determined by inductively coupled plasma atomic emission spectroscopy (ICP-AES) of acid-digested samples. The amount of Cd^{2+} in the CdS nanorod solution in each reaction was between 1×10^{-6} to 1×10^{-5} moles. The salt tetrakis(acetonitrile)copper(I) hexafluorophosphate ($[MeCN]_4Cu(I)PF_6$) was used as the weak

binding affinity of the anion makes the salt readily soluble in methanol such that the Cu^+ solution is miscible with the colloidal solution of nanorods dispersed in toluene. In a typical reaction, 12 mg of ($[MeCN]_4Cu(I)PF_6$) was dissolved in 2.5 mL of methanol (MeOH). This solution was used for full conversion or was further diluted five or ten-fold for partial conversion. For full conversion, the $[MeCN]_4Cu(I)PF_6$ solution (~ 0.6 to 1 mL) was added to a stirring solution of CdS nanorods in toluene (~ 2 mL). For partial conversion a concentrated solution of CdS nanorods in toluene (~ 50-500 μL) was added to a stirring $[MeCN]_4Cu(I)PF_6$ solution (~ 0.1 – 1 mL) diluted in toluene (~ 2 mL). The color of the nanocrystal solution changes rapidly (< 1 second) from yellow to golden brown after mixing of the Cu^+ and CdS solutions, and the nanorods were washed by the addition of MeOH followed by centrifugation and removal of the supernatant. To examine the effect of slow addition of Cu^+ ions, the $[MeCN]_4Cu(I)PF_6$ solution was loaded in a syringe pump and added at a rate of 0.15 mL/min via a capillary needle to a stirring solution of CdS nanorods in toluene. The Supporting Information details the specific reaction conditions used to produce the CdS-Cu_2S and Cu_2S nanorods characterized in this work.

III. Characterization. Bright field TEM images were obtained using a Tecnai G2 S-Twin electron microscope operating at 200 kV. TEM samples were prepared by placing a drop of the nanocrystal solution onto a carbon-coated copper grid in ambient atmosphere. The elemental distribution of the nanocrystals was characterized by energy-filtered transmission electron microscopy (EFTEM). The EFTEM experiments were performed using a Philips CM200 microscope or a Tecnai microscope equipped a high-angle annular dark field (HAADF) detector. Both microscopes were equipped with a field emission gun, an electron energy loss spectrometer and a Gatan Image Filter (GIF) and were operated at 200 kV. The elemental maps were obtained by using the three-window method.[23] The Cd M-edge (404 eV) and Cu L-edge (931 eV) were used for the three-window mapping to make the color composite images. The color composites of Cd and Cu-EFTEM images were made using Image-Pro Plus software. The Cu M-edge (120 eV, minor) was used for the Cu energy-filtered images.

Statistics for the length and diameter of the initial CdS nanorods and fully converted Cu_2S nanorods were gathered from bright field TEM images using Image-Pro Plus software, and at least 250 measurements were made for each sample. Statistics for the segment lengths of the CdS and Cu_2S regions in the binary nanorods were determined from EFTEM making at least 150 measurements. The degree of asymmetry for each CdS-Cu_2S binary nanorod was taken to be one minus the ratio of the length of the short Cu_2S segment over the length of the long Cu_2S segment. Using this definition, a nanorod possessing two Cu_2S segments of equal lengths has an asymmetry value of 0, and a nanorod with Cu_2S on only one side of the nanorod has an asymmetry value of 1. The length fraction of the nanorod converted to Cu_2S was measured as the ratio of the combined length of Cu_2S segments over the total length of the nanorod. Thus, a nanorod that is entirely composed of CdS will have a length conversion of 0, and a nanorod fully converted to Cu_2S will have a value of 1. The CdS-Cu_2S interfaces were grouped into three categories: flat and parallel to the nanorod cross-section, flat and at an angle to the cross-section, and multifaceted (which appear curved in low-magnification TEM images). Because the apparent angle and curvature of an interface depends on its relative orientation on the TEM substrate, the fraction of each of these types of interfaces (measured from a population of > 200 nanorods) is approximate.

The crystal structure of the samples was measured from powder X-ray diffraction (XRD) obtained on a Bruker AXS diffractometer using Co Kα radiation (1.790 Å) and a general area detector. The instrument resolution was 0.05° in 2θ, and the acquisition time for each sample was one hour. XRD samples were prepared by dissolving the precipitated nanocrystals in a minimal amount of toluene or chloroform and using a capillary tube to drop the solution onto a glass sample plate.

IV. Ab initio Calculations. Supercell geometries for CdS-Cu_2S epitaxial attachments were studied using the VASP program, a density functional theory (DFT) code using planewaves and pseudopotentials.[24,25] The generalized gradient approximation (GGA) was used for the exchange-

correlation part, along with projector augmented wave (PAW) pseudopotentials, and planewave energy cutoffs of 280 eV. We used Γ-point only eigenenergies in the Brillouin zone as the supercells are sufficiently large to ensure weak dispersion of energy bands. All geometries were relaxed to have the forces on atoms reduced to 0.01 eV/Å or less. CdS-Cu_2S interface formation energies for epitaxial connections between different facets of the two crystals were computed analogously to our previous calculations for the CdS-Ag_2S system where the interface formation energy is defined as the *ab initio* total energy difference of the supercell containing the interface and its bulk constituents.[21] Total formation energies containing both chemical and elastic contributions were obtained by using the difference in energy between the supercell and natural bulk structures. To calculate the chemical energy alone, the bulk lattices were strained similar to the lattice in the supercell. The elastic contributions were computed assuming the distortions occurred in the Cu_2S or Ag_2S cell only to match to the lattice of the CdS cell. The cell thicknesses for Cu_2S were 13.5 Å for the end-on and angled attachments to CdS and 27.3 Å for the side attachment. CdS-Ag_2S interface formation energies for similar end-on connections to the CdS nanorods were previously calculated,[21] and an additional side attachment was modeled for this work. The cell thicknesses for Ag_2S were 13.7 Å in all cases.

RESULTS

I. Structural Characterization of CdS-Cu_2S Binary Nanorods

X-ray diffraction (XRD) patterns of the CdS nanorods before and after the addition of increasing amounts of Cu^+ cations are shown in Figure 1. The addition of excess Cu^+ cations relative to the amount of Cd^{2+} within the wurtzite CdS nanocrystals leads to their complete transformation to the low-temperature form of chalcocite Cu_2S as measured from XRD patterns of the reactant and product nanorods (Figure 1 and Supplemental Figure 1).[26] Partially converted samples made by substoichiometric addition of Cu^+ ions show a combination of diffraction peaks from both CdS and

Cu_2S. Peaks belonging to the CdS phase disappear and peaks belonging to Cu_2S grow stronger in intensity with increasing amounts of Cu^+ added to the solution of CdS nanorods. The bright field transmission electron microscopy (TEM) images in Figure 2 show that after complete Cu^+ cation exchange, the shape and size of the nanorods is preserved within the 8% contraction in lattice volume upon conversion from CdS to Cu_2S.

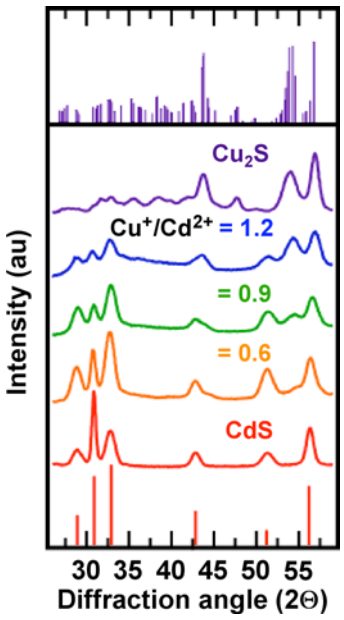

Figure 1. XRD patterns of initial CdS nanorods (bottom, red) and CdS-Cu_2S binary nanorods formed with increasing amounts of Cu^+. The addition of excess Cu^+ cations leads to full conversion of the wurtzite nanorods into the low temperature phase of chalcocite Cu_2S. The Cu^+/Cd^{2+} cation ratio used for the partial exchange reactions is provided above each plot. Patterns from the Joint Committee on Powder Diffraction Standards (JCPDS) for wurtzite CdS (bottom, JCPDS #00-041-1049, space group P63mc (186)) and low temperature chalcocite Cu_2S (top, JCPDS # 00-033-0490, space group P21/c (14)) are included for reference.

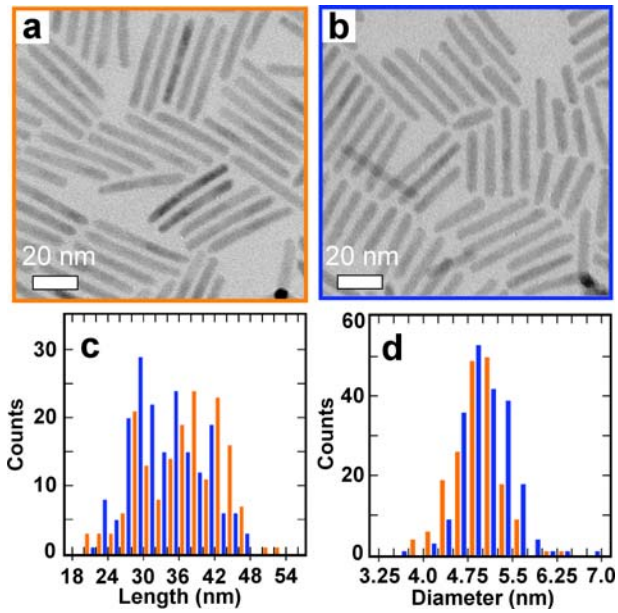

Figure 2. (a) TEM image of initial CdS nanorods and (b) Cu_2S nanorods after complete Cu^+ exchange, showing shape preservation of the nanorods. (c) Length distributions of the nanorods before (orange) and after (blue) cation exchange and (d) diameter distributions of the nanorods.

For partial Cu^+ exchange, energy-filtered TEM (EFTEM) was used to obtain elemental mappings of the Cu- and Cd-containing regions of binary nanorods. The composite energy-filtered image in Figure 3 clearly shows the CdS and Cu_2S portions of the binary nanorods, where the ends of the nanorods have been converted to Cu_2S (see Supplemental Figure 2 for the original Cd- and Cu-EFTEM images used to make the color composite). The preferential conversion of the ends of the nanorods occurs for varying lengths, diameters, and aspect ratios. Observing nanorods with different fractions of conversion to Cu_2S, the EFTEM images indicate that cation exchange starts at the ends, and the Cu_2S regions grow into the nanorods upon further exchange. The only cases where Cu_2S segments existed in between regions of CdS were at sites of irregularities such as kinks along the nanorod diameter or at the zinc-blende branch-point of bipod and tripod nanocrystals.[27]

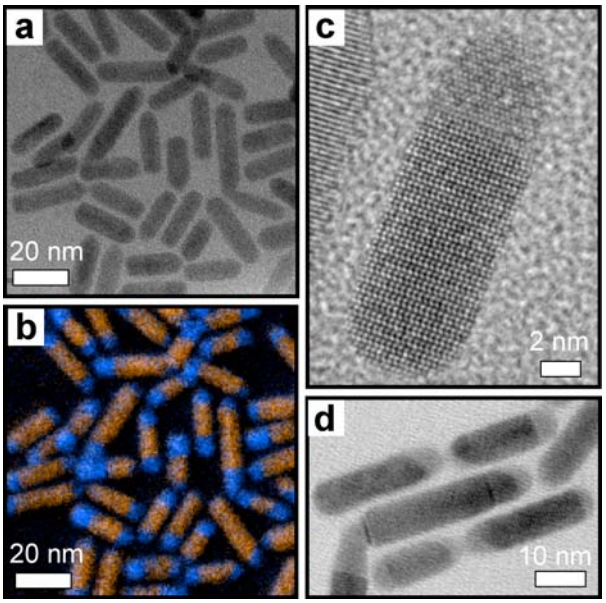

Figure 3. TEM images of CdS-Cu_2S binary nanorods. (a) bright-field (zero-loss) image. (b) color-composite EFTEM image, where the orange regions correspond to the Cd energy-filtered mapping and blue regions correspond to the Cu mapping. (c) High-resolution TEM image of a CdS-Cu_2S nanorod. (d) Brightfield TEM image, where CdS-Cu_2S interfaces can be seen at various angles relative to the nanorod cross-section.

The high-resolution TEM (HRTEM) image of a Cu_2S-CdS heterostructure in Figure 3c shows the epitaxial interface between the two materials within the nanorod.[28] The majority of interfaces are flat and parallel to the cross-section of the nanorod (parallel to the (0001) plane of CdS). However, a significant population of interfaces (up to 30% in various samples) are at an angle up to ~ 40° relative to the nanorod cross-section (see Figure 3d). As the apparent angle of the interface depends on the relative orientation of the nanorod on the TEM substrate, it is likely that these interfaces occur along specific crystallographic facets of the two lattices, rather than at a continuous range of angles. Some interfaces observed by HRTEM consist of multiple facets and appear curved at lower-magnifications. Step-edges

were also observed in some interfaces, which naturally arise if only a portion of cations within an atomic layer is exchanged.

While Cu^+ cation exchange occurs at both ends of the CdS nanorods, the relative lengths of the two Cu_2S end segments within a given nanorod can vary significantly. As the CdS wurtzite lattice lacks inversion symmetry, the (0001) and $(000\bar{1})$ end facets of the nanorods are crystallographically nonequivalent.[27] Cd atoms at a $(000\bar{1})$ surface facet expose three dangling bonds whereas Cd atoms at a (0001) surface expose only one dangling bond. Thus, the bonding arrangement of Cd atoms to the interfacial sulfur layer at the CdS-Cu_2S attachment will be different at opposite ends of the nanorod. Two important factors found to affect the asymmetry of the Cu_2S end segments are the shape (curvature and diameter) of the ends of the CdS nanorods and the rate of addition of the Cu^+ ions to the CdS solutions.

Figure 4 shows Cu-EFTEM images for three CdS-Cu_2S binary nanorod samples along with histograms of the asymmetry of the length of the Cu_2S segments within individual nanorods for each of the samples shown. To examine the effect of the nanocrystal dimensions on the asymmetry of Cu_2S segments, partial Cu^+ exchange was performed on nanorods of different lengths and diameters. Sample 1 shown in Figure 4a used CdS nanorods with an average length of 48±7 nm (average ± first standard deviation) and a diameter of 6±0.8 nm. The molar ratio of Cu^+ cations relative to Cd^{2+} was 0.51. In this case, the Cu_2S segment lengths are symmetric, evident by the continual decrease in counts in the asymmetry histogram in Figure 4d from 0 to 1. The mean asymmetry for this sample was 0.25 where the asymmetry of the two Cu_2S segments in a given binary nanorod is defined as one minus the ratio of the length of the short segment length over the length of the long segment. In sample 2 shown in Figure 4b, which used CdS nanorods with a smaller average length but larger diameter (length = 29±4 and diameter = 9±0.8 nm) and a Cu^+/Cd^{2+} ratio of 0.56, the reaction produced asymmetric heterostructures as the counts in the asymmetry histogram tend to increase from 0 to 1 (mean asymmetry = 0.6). As seen in

Figure 4, a significant difference between the two nanorod samples is that the ends of smaller diameter nanorods in sample 1 possess higher curvature (meaning the are composed of multiple surface facets). This appears to lead to a higher fraction of curved (multifaceted) interfaces in sample 1 (~18%) compared to sample 2 (~2 %). On the other hand, there appears to be no correlation between the asymmetry of the Cu_2S segments and the length of the nanorods.

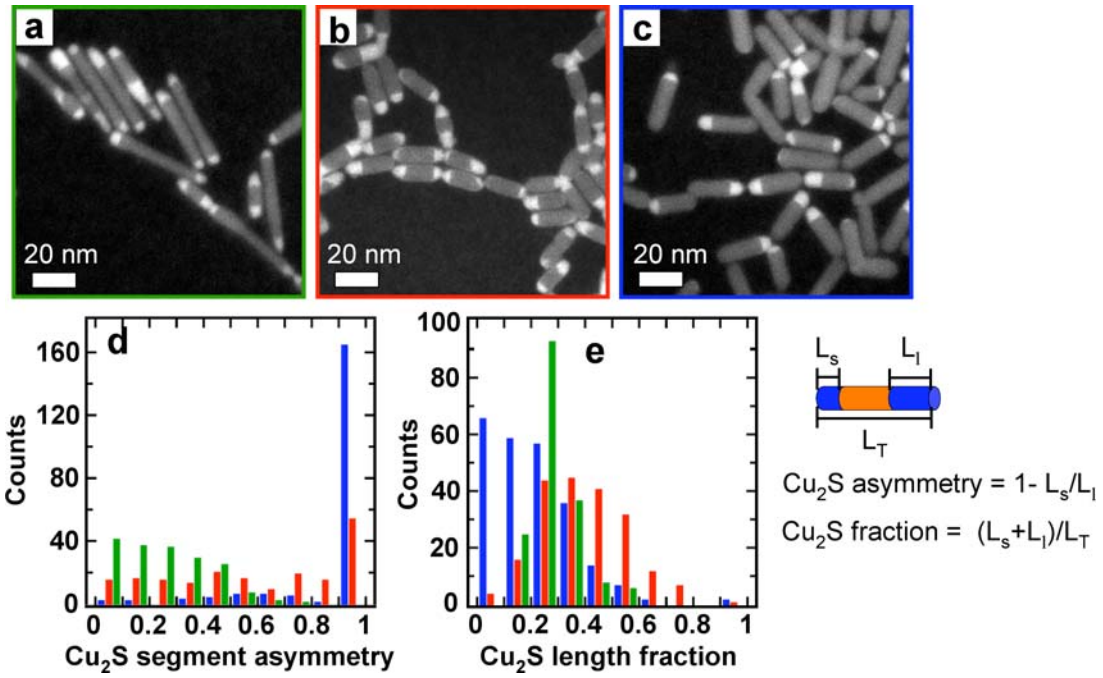

Figure 4. Cu-EFTEM images of CdS-Cu_2S binary nanorods and corresponding size statistics of the Cu_2S and CdS regions. The bright regions in the images correspond to Cu_2S and the grey regions to the CdS portions of the nanorods. The green, red, and blue bars in the histograms correspond to samples 1, 2, and 3 shown in (a), (b), and (c), respectively. The three samples were made under the following conditions: (a) sample 1: initial CdS nanorods with dimensions of 48×6 nm and fast addition to the Cu^+ solution, (b) sample 2: CdS nanorods with dimensions of 29×9 nm and fast addition to the Cu^+ solution, and (c) sample 3: The same initial nanorods as 2, but with slow addition of Cu^+ ions. (d) Histograms of the asymmetry of the Cu_2S segment lengths on the ends of the nanorods for the three samples. (e)

Histograms of the Cu_2S length fraction within the binary nanorods. The asymmetry and length fraction of the Cu_2S segments are defined to the right.

Sample 3 used the same initial nanorods as sample 2, but the Cu^+ solution was added drop wise via a syringe pump to the CdS solution. Slowing the rate of addition of Cu^+ cations to the CdS nanorods has several significant effects on the morphology of the CdS-Cu_2S heterostructures. First, it greatly enhances the asymmetry of the heterostructures leading to a majority of nanorods with Cu_2S only on one end as shown in Figure 4c (sample 3, mean asymmetry = 0.91). It also widens the distribution of the fraction exchanged among the individual nanorods within sample 3 (see Figure 4e). Thus, the disparity of Cu_2S segment sizes both within individual nanorods and among the different nanorods in a sample increases from sample 1 to 2 to 3. Finally, sample 3 has fewer nanorods with interfaces that are at an angle to the cross-section of the nanorod (~15% for sample 3 versus ~30% for sample 2). Thus, the slow addition of Cu^+ cations appears to increase the selectivity for nucleation of one CdS-Cu_2S interface per nanorod that is parallel to the nanorod cross-section.

II. Modeling of the CdS-Cu_2S epitaxial attachment

The nucleation and growth of Cu_2S within a CdS nanocrystal involves complex atomic motions making the microscopic mechanism for this solid-state reaction relatively difficult to model. However, the formation energies for CdS-Cu_2S interfaces created at different facets of the CdS crystal give a measure of their relative stability, where interfaces with low formation energies should be observed more frequently. We constructed models of epitaxial connections between different facets of wurtzite CdS and chalcocite Cu_2S shown in Figure 5, which were used to calculate interface formation energies, defined as the total energy difference of the supercell containing the interface and its bulk constituents. The values are presented in Table 1, along with interface formation energies for CdS-Ag_2S attachments previously calculated using the same method.[21] Table 1 includes both chemical formation energies,

reflecting the strength of interfacial Cd-S-Cu (Cd-S-Ag) bonds, as well as the elastic contribution due to lattice distortions from the epitaxial mismatch. While the value of the interfacial strain energy depends on the thickness of the Cu_2S (Ag_2S) cells used in the calculation, a comparison of the elastic contributions is useful, as strain has been shown to play an important role in forming the striped pattern observed in CdS-Ag_2S heterostructures produced by cation exchange.[1,21]

Table 1. Interface formation energies (in eV/per interface unit containing one S atom) for attachments of CdS to Cu_2S or Ag_2S. The lattices and facets comprising each interface are listed. The chemical contribution to the formation energy along with the sum of the chemical and elastic contributions are provided for each interface. The elastic contributions were computed assuming the distortions occurred in the Cu_2S or Ag_2S only to match the lattice of the CdS. The thicknesses of the Cu_2S cells were 13.5 Å for the end-on and angled attachments and 27.3 Å for the side attachment. The Ag_2S thicknesses for were 13.7 Å in all cases.

	End-on CdS ±(0001)[a] to orthorhombic Cu_2S ±(001) $(I_1 + I_2)/2$	End-on CdS (000$\bar{1}$) to orthorhombic Cu_2S (001) (I_1 only)	End-on CdS (0001) to orthorhombic Cu_2S (001) (I_2 only)	Angled CdS ±(10$\bar{1}$2) to monoclinic Cu_2S ±(001)	Side CdS ±(10$\bar{1}$0) to orthorhombic Cu_2S ±(001)	End-on CdS ±(0001) to orthorhombic Ag_2S ±(001)[b]	End-on CdS ±(0001) to orthorhombic Ag_2S ±(100)[b]	Side CdS ±(10$\bar{1}$0) to orthorhombic Ag_2S ±(001)
Chemical	0.204	0.116	0.292	0.348	0.83	-0.3	-0.87	-1.15
Chemical + elastic	0.255	0.161	0.349	0.416	0.85	1.51	1.57	2.81

[a] The ± symbol indicates that facets with opposite (hkl) or (hkil) indexes comprise the two interfaces in the supercell.

[b] Values calculated in reference [21]

As the hexagonal close-packed (hcp) sulfur sublattices in CdS and Cu_2S are crystallographically nearly identical,[29] epitaxial attachments can be made by aligning the sulfur lattices of the two crystals. While the unit cell of low chalcocite is monoclinic, it is common to model it as pseudo-orthorhombic, to make the symmetry of the lattice easier to visualize (see Supplemental Figure 3).[26,30] To align the c-axes

of the hcp sulfur lattices, the [001] axis of the orthorhombic Cu_2S cell is made parallel with the [0001] axis of the hexagonal CdS lattice. The attachment of orthorhombic Cu_2S to the $(000\bar{1})$ and (0001) end facets of CdS naturally creates interfaces parallel to the cross-section of the nanorod as shown in Figure 5a. However, because the CdS lattice lacks inversion symmetry about the c-axis, these two interfaces have different epitaxies, which are labeled as I_1 and I_2. In the interface I_1, connecting Cu_2S to the $(000\bar{1})$ CdS facet, each Cd atom bonds to three S atoms in the interfacial layer. While in the interface, I_2, connecting Cu_2S to the (0001) CdS facet, each Cd atom has one bond to an interfacial S atom.

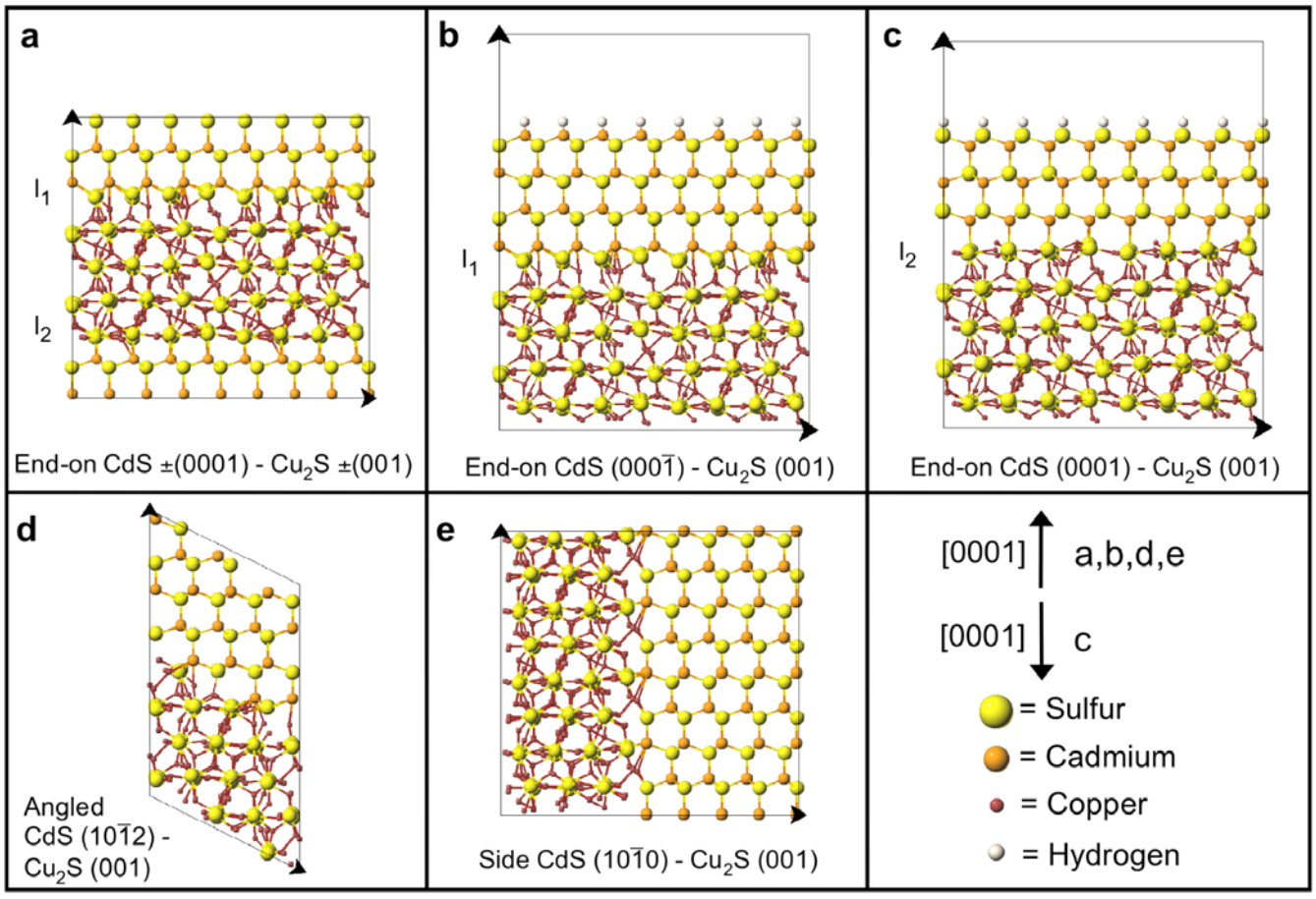

Figure 5. Models of the CdS-Cu_2S epitaxial attachments corresponding to the interface formation energies listed in Table 1. (a) End-on, CdS-Cu_2S attachment using the Cu_2S orthorhombic cell. This supercell contains two non-equivalent interfaces labeled as I_1 and I_2. (b) Supercell containing I_1 only connecting Cu_2S to the $(000\bar{1})$ CdS facet and (c) supercell containing I_2 connecting Cu_2S to the (0001)

facet of CdS. These two supercells also possess CdS and Cu_2S surfaces, which are subtracted out to separate the formation energies for I_1 and I_2. (d) Angled, CdS-Cu_2S interface formed with the original monoclinic Cu_2S lattice connecting to hexagonal CdS. (e) Side, CdS-Cu_2S interface connecting orthorhombic Cu_2S to the $(10\bar{1}0)$ facet of the CdS nanorod.

The supercell geometry used to calculate the interface formation energies implies infinite repetition of alternating CdS and Cu_2S slabs, such that two interfaces are always present. In the case of the supercell in Figure 5a, where the bonding arrangement of Cd atoms in the interfacial layer are significantly different for the two attachments, it is necessary to separate their formation energies. The detailed procedure for determining the individual energies of these two interfaces is provided in the Supporting Information. Briefly, we construct supercells, shown in Figures 5b and 5c, which contain a single interface (I_1 or I_2), the opposite CdS surface passivated by pseudo-hydrogen,[31] and the opposite Cu_2S surface left unpassivated in vacuum. By taking the difference between the formation energies of these two supercells, the Cu_2S surface energies cancel out,[32] leaving the difference in energy between I_1 and I_2 along with the CdS (0001) and $(000\bar{1})$ surface energies. The CdS surfaces can be subtracted out using auxiliary CdS cells (shown in Supplementary Figure 5). Combining the energy difference between I_1 and I_2 with their average determined from the supercell in Figure 5a leads to the desired individual formation energies for connected attached to the wurtzite CdS (0001) or $(000\bar{1})$ facets. As seen in Table 1, the interface I_1 has a chemical formation energy that is about 2.5 times lower than I_2.

Due to the small lattice mismatch between the sulfur lattices of CdS and Cu_2S, the formation energies are determined primarily by the distributions of Cu and Cd atoms at the interface. The optimal geometry for metal atoms bonded to the interfacial layer of sulfur atoms should satisfy local electron counting rules, i.e. each S atom should have a local environment that supplies two electrons in order to fill the sulfur 3*p* bands (see Supporting Information for further detail). While the Cu atoms are

somewhat disordered in the interfaces I_1 and I_2, it can be seen that they form layers parallel to the interface, making it relatively easy to move Cu atoms from one layer to another. By moving four Cu atoms from the Cu layer at interface I_1 to that of I_2 local electron counting is satisfied. However, this is not true for the other CdS-Cu_2S epitaxial connections that we modeled. Due to the relative orientation of the Cu atomic layers in the two interfaces described below we were not able to satisfy local electron counting rules, which contributes to their higher formation energies.

By using the original monoclinic lattice for chalcocite Cu_2S, the sulfur lattices can be matched by connecting the ±(001) facets of Cu_2S to the ±(10$\bar{1}$2) facets of CdS. This interface appears at an angle of ~35° to the nanorod cross-section when viewed along the [100] direction of the Cu_2S lattice, and the apparent angle of the interface will vary with its orientation on the TEM substrate.[33] Not only does the hexagonal-monoclinic interface have a larger formation energy than I_1 and I_2, but it also produces a greater total interfacial area. Only a minority of the interfaces observed were at an angle to the cross-section (< 30 % for fast addition and < 15 % for slow addition of Cu^+). We also modeled the attachment of orthorhombic Cu_2S to the ±(10$\bar{1}$0) side facets of the CdS nanorod as shown in Figure 5e.[34] This interface has a significantly greater formation energy than the other three connections, and Cu_2S regions were rarely observed on the sides of the nanorods. This is unlike Ag^+ exchange of CdS nanorods, where small Ag_2S regions form on both the sides and ends of the CdS nanorods in the initial stages of the reaction.

DISCUSSION

I. Comparison of Cu^+ and Ag^+ cation exchange

The heterostructure morphologies for different conversion fractions of the CdS nanorods to Cu_2S or Ag_2S aid in elucidating the movement of the reaction fronts during cation exchange within the nanocrystals.[21] Figure 6 provides a general schematic of the changes in morphology of the CdS-Cu_2S

and CdS-Ag_2S binary nanorods as the Cu^+/Cd^{2+} or Ag^+/Cd^{2+} ratio increases (for partial exchange the cation ratio is between 0 and 2). A comparison of the chemical formation energies listed in Table 1 to the heterostructures observed at different fractions of exchange illustrates that the lower the chemical formation energy of an interface, the more frequently that interface is observed at low fractions of Cu^+ or Ag^+ exchange. The chemical contributions to the formation energy are negative for all of the CdS-Ag_2S interfaces, while they are positive for each of the CdS-Cu_2S interfaces. This difference can be partially understood by comparing the bonding character and atomic structure in Cu_2S and Ag_2S. It can be shown that the Cu-S bonds exhibit more ionic character compared to Ag-S bonds, resulting in weaker bonding at the interface, and therefore a higher formation energy. Furthermore, while the positions Ag atoms at the CdS-Ag_2S interface are close to the optimal bulk positions, relatively large rearrangements of Cu atoms are needed in order for them to connect to the interfacial sulfur layer. Such rearrangements increase the formation energy of the CdS-Cu_2S interface.

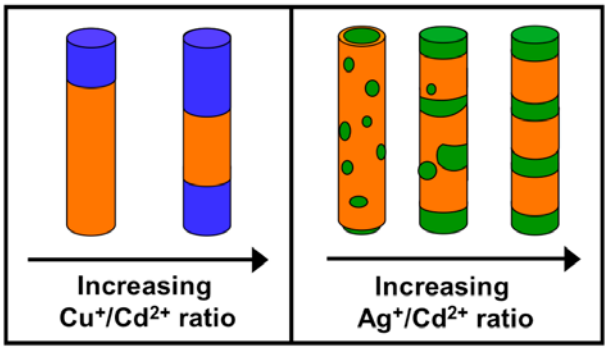

Figure 6. Development of the morphology of binary nanorods produced by cation exchange for increasing amounts of Cu^+ or Ag^+ added to CdS nanorods.

The negative chemical formation energies of the three CdS-Ag_2S attachments favor the creation of Cd-S-Ag interfacial bonds on both the ends and sides of the CdS nanorods. This leads to non-selective nucleation over the entire surface of the nanorod, forming small Ag_2S dots inside the CdS lattice when low amounts of Ag^+ are added ($Ag^+/Cd^{2+} < 0.5$).[1,21] In the CdS-Cu_2S system where the

chemical formation energies are all positive, the Cu_2S attachments to the ends of the nanorods possess the lowest formation energies and are the predominant interfaces in the heterostructures. The angled attachment connecting the basal facets of the monoclinic Cu_2S lattice to CdS has both a higher chemical formation energy per interfacial unit and produces a greater interfacial area. Thus, this interface occurs at a significantly lower frequency, particularly in the case where the Cu^+ ions are slowly added to the CdS solution. Finally, growth of Cu_2S on the sides of the CdS nanorods is rarely observed, which correlates with the calculated chemical formation energy that is approximately seven times greater than that of end-on connection to the $(000\bar{1})$ CdS facet.

As the interfacial area increases, the elastic energy become a more important contribution, such that interfaces with a lower total formation energy (chemical + elastic) are dominant. The large lattice mismatch between the CdS and Ag_2S lattices drives coalescence of the Ag_2S regions in order to minimize the amount of interfacial area as they grow into the nanorods. During this process, interfaces connecting Ag_2S to the $(10\bar{1}0)$ type side facets of CdS are less stable as they possess a greater elastic energy compared to interfaces connecting to the ±(0001) facets. The system removes these high energy interfaces when the Ag_2S regions grow to span the entire diameter of the nanorod, leaving only interfaces parallel to the cross-section of the nanorod (see Figure 6b). This process leads to a striped pattern of alternating CdS and Ag_2S segments. On the other hand, in the Cu_2S-CdS system where there is little lattice mismatch between the sulfur lattices of the two crystals, the Cu_2S regions grow in from either end of the nanorod until they merge in the middle. The initial nucleation of CdS-Cu_2S interfaces at the ends of the nanorods is a low-energy configuration that is maintained as the exchange front moves along the length of the nanorod. Thus, the basic morphology of the nanorods possessing Cu_2S segments at one or both ends is the same for different conversion fractions.

II. Asymmetry of Cu^+ cation exchange

The relative activation barriers for nucleation at each end of the nanorod control the asymmetry of the Cu_2S segments. In principle, disparate rates of diffusion of cations in opposite directions along the nanorod could also contribute to asymmetric growth. However, previous kinetic studies of cation exchange suggest that interface nucleation provides the main kinetic barrier for transformation of the nanocrystal.[35] The chemical formation energy for the Cu_2S attachment to the CdS $(000\bar{1})$ facet (I_1) is lower by ~0.18 eV per Cd-Cu-S unit compared to attachment to the (0001) facet (I_2). Moreover, the $(000\bar{1})$ end facet of the CdS nanocrystal is believed to be the least stable surface of the nanorod as Cd atoms possess three dangling bonds, making full passivation difficult without significant restructuring of the surface atoms.[36] Therefore, the connection of orthorhombic Cu_2S to the $(000\bar{1})$ end of the nanorods produces the thermodynamically most stable configuration as it both removes a high-energy surface and creates the lowest energy interface. This suggests that the asymmetric CdS-Cu_2S nanorods are produced by selective nucleation of Cu_2S at the $(000\bar{1})$ end of the nanorod

The increased asymmetry of Cu_2S segments in sample 2 over sample 1 as shown in Figure 4 is attributed to the larger diameter and flatter ends of the initial CdS nanorods used to produce sample 2. The shape of the CdS nanorods is kinetically-determined during their growth by the relative rates of monomer addition along different crystallographic directions of the particle.[27,37] Under the non-equilibrium growth conditions used to produce highly anisotropic nanocrystals, the $(000\bar{1})$ and (0001) ends of the nanorods are partially replaced by the more stable $\{10\bar{1}1\}$ type facets leading to pencil or arrow-shaped nanorods.[27] The epitaxy of the nucleating interface during cation exchange will depend on the surface area of the different crystalline facets exposed. The binary nanorods in sample 1 (Figure 4a) in which the initial nanorods ends have a higher curvature compared to those used to make sample 2 (Figure 4b) also have a higher fraction of curved interfaces. Nanorods with multi-faceted (curved) end faces expose less of the (0001) and $(000\bar{1})$ surfaces, which may lower the selectivity for interface

nucleation at one end. Furthermore, a larger diameter will accentuate the difference in total formation energy between I_1 and I_2. As larger diameter nanorods generally also possess flatter ends, these two parameters act in concert to increase the asymmetry of the Cu_2S segment lengths.

Maintaining a low concentration of Cu^+ ions present in solution during the exchange reaction enhances the formation of a single interface in each binary nanorod. This can be seen as the asymmetry of Cu_2S segments greatly increases for slow (sample 3, Figure 4c) versus fast (sample 2, Figure 4b) addition of Cu^+ cations to the same initial batch of CdS nanorods. In addition, the percentage of interfaces at an angle to the nanorod cross-section decreases for slow addition. However, the distribution of the fraction converted to Cu_2S among individual nanorods widens, indicating that nucleation and growth of Cu_2S become increasingly overlapped in time. This is expected as the concentration of Cu^+ cations during the early stages of the drop-wise addition is not enough for nucleation to occur on all of the nanorods at once. Previous studies on the reaction kinetics of Ag^+ cation exchange in CdSe nanocrystals support a mechanism where once an interface nucleates in a nanocrystal by cation exchange at the surface, the kinetic barrier for further exchange is relatively low.[35] Thus, upon slow addition of Cu^+ ions, exchange will occur more rapidly at CdS-Cu_2S interfaces that have already formed over the creation of new interfaces, widening the distribution of the Cu_2S fraction among the nanorods. The temporal separation of nucleation and growth stages is often used to achieve monodisperse colloidal nanostructures.[22,38] In the present case we have attempted only rapid addition of the CdS and Cu^+ solutions or slow injection of Cu^+ at a constant rate. With further optimization of the rate of Cu^+ addition throughout the course of the reaction it may be possible to maximize the selectivity for nucleation on the $(000\bar{1})$ facet while also separating the nucleation and growth stages to yield a narrow distribution of Cu_2S within the nanorods.

CONCLUSIONS

We have demonstrated that the crystallographic selectivity for cation exchange to occur at different facets of ionic nanocrystals plays a critical role in determining the morphology of the resulting nanocrystal heterostructures. The preferential nucleation and growth of Cu_2S at the ends of CdS nanorods during Cu^+ exchange is attributed to the high stability of CdS-Cu_2S interfaces formed at these facets. In comparison, non-selective nucleation in Ag^+ exchange leads to the formation of multiple Ag_2S regions within the nanorod. The differences between these two systems lie in both the chemical favorability for creating interfacial bonds as well as the elastic distortions between attachments connecting various facets of the two materials. The relative stabilities of the interfaces we have modeled correspond well with the frequency that the corresponding morphologies are observed. In the future, similar modeling of the epitaxy in nanoscale heterostructures may be applied to other material pairs to predict which interfaces will be the most stable. As both the shape and size of the nanocrystals determine the crystallographic facets exposed at the surface, these parameters can be used to control the nanocrystal's reactivity. Selective facet reactivity can in turn provide tunability of the physical properties of nanocrystal heterostructures through control of the spatial arrangement of their components.

ACKNOWLEDGMENT

This work was supported by the Director, Office of Science, Office of Basic Energy Sciences, of the U.S. Department of Energy under Contract No. DE-AC02-05CH11231. The synthetic chemistry was developed under funding through the Helios Solar Energy Research Center at Lawrence Berkeley National Laboratory (LBNL). The theoretical modeling used computational facilities at the National

Energy Research Scientific Computing Center (NERSC) at LBNL. EFTEM imaging was performed at the National Center for Electron Microscopy (NCEM) at LBNL. H. Zheng thanks M. Watanabe, Z. Lee and C. Song for their advice on EFTEM imaging. D. O. Demchenko thanks W. L. Lambrecht and P. Lukashev for providing the atomic structure for high temperature chalcocite. The authors thank R. Robinson for useful discussions.

SUPPORTING INFORMATION PARAGRAPH

The supporting information includes the following information: protocols for the synthesis of the CdS nanorods and CdS-Cu_2S binary nanorods characterized in this work, a description of different phases of bulk Cu_2S, a discussion of electron counting rules for interfacial atoms in the CdS-Cu_2S interfaces I_1 and I_2, and a derivation of the individual formation energies for I_1 and I_2. The following figures are also provided: XRD simulations for the chalcocite and djurleite phases of bulk Cu_2S, the original Cd- and Cu-EFTEM images used to make the color composite image in Figure 3b, a schematic of the relation between monoclinic and orthorhombic cells of Cu_2S, the original supercell used to calculate the interface energy of the side attachment of Cu_2S to CdS, and auxiliary CdS structures used to determine the individual interface formation energies for I_1 and I_2.

TOC graphic

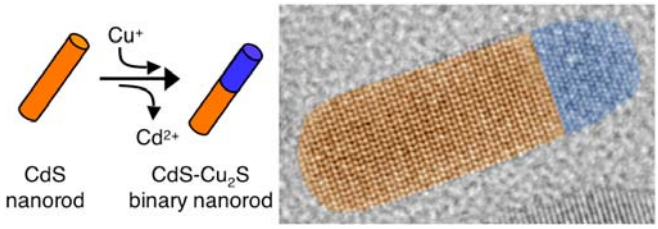

REFERENCES

(1) Robinson, R. D.; Sadtler, B.; Demchenko, D. O.; Erdonmez, C. K.; Wang, L.-W.; Alivisatos, A. P.

Science **2007**, *317*, 355-358.

(2) Yin, Y.; Alivisatos, A. P. *Nature* **2005**, *437*, 664-670.

(3) Jun, Y.-W.; Choi, J.-S.; Cheon, J. *Chemical Communications* **2007**, 1203-1214.

(4) Cozzoli, P. D.; Pellegrino, T.; Manna, L. *Chemical Society Reviews* **2006**, *35*, 1195-1208.

(5) Casavola, M.; Buonsanti, R.; Caputo, G.; Cozzoli, P. D. *European Journal of Inorganic Chemistry* **2008**, *6*, 837-854.

(6) Shi, W.; Zeng, H.; Sahoo, Y.; Ohulchanskyy, T. Y.; Ding, Y.; Wang, Z. L.; Swihart, M.; Prasad, P. N. *Nano Letters* **2006**, *6*, 875-881.

(7) Milliron, D. J.; Hughes, S. M.; Cui, Y.; Manna, L.; Li, J.; Wang, L.-W.; Alivisatos, A. P. *Nature* **2004**, *430*, 190-195.

(8) Mokari, T.; Rothenberg, E.; Popov, I.; Costi, R.; Banin, U. *Science* **2004**, *304*, 1787-1790.

(9) Kudera, S.; Carbone, L.; Casula, M. F.; Cingolani, R.; Falqui, A.; Snoeck, E.; Parak, W. J.; Manna, L. *Nano Letters* **2005**, *5*, 445-449.

(10) Shieh, F.; Saunders, A. E.; Korgel, B. A. *Journal of Physical Chemistry B* **2005**, *109*, 8538-8542.

(11) Talapin, D. V.; Nelson, J. H.; Shevchenko, E. V.; Aloni, S.; Sadtler, B.; Alivisatos, A. P. *Nano Letters* **2007**, *7*, 2951-2959.

(12) Sun, Y.; Xia, Y. *Science* **2002**, *298*, 2176-2179.

(13) Yin, Y.; Rioux, R. M.; Erdonmez, C. K.; Hughes, S.; Somorjai, G. A.; Alivisatos, A. P. *Science* **2004**, *304*, 711-714.

(14) Cable, R. E.; Schaak, R. E. *Journal of the American Chemical Society* **2006**, *128*, 9588-9589.

(15) Mews, A.; Eychmuller, A.; Giersig, M.; Schooss, D.; Weller, H. *Journal of Physical Chemisty* **1994**, *98*, 934-941.

(16) Dloczik, L.; Koenenkamp, R. *Journal of Solid State Electrochemistry* **2004**, *8*, 142-146.

(17) Son, D. H.; Hughes, S. M.; Yin, Y.; Alivisatos, A. P. *Science* **2004**, *306*, 1009-1012.

(18) Wark, S. E.; Hsia, C.-H.; Son, D. H. *Journal of the American Chemical Society* **2008**, *130*, 9550-

9555.

(19) Camargo, P. H. C.; Lee, Y. H.; Jeong, U.; Zou, Z.; Xia, Y. *Langmuir* **2007**, *23*, 2985-2992.

(20) Pietryga, J. M.; Werder, D. J.; Williams, D. J.; Casson, J. L.; Schaller, R. D.; Klimov, V. I.; Hollingsworth, J. A. *Journal of the American Chemical Society* **2008**, *130*, 4879-4885.

(21) Demchenko, D. O.; Robinson, R. D.; Sadtler, B.; Erdonmez, C. K.; Alivisatos, A. P.; Wang, L.-W. *ACS Nano* **2008**, *2*, 627-636.

(22) Peng, Z. A.; Peng, X. *Journal of the American Chemical Society* **2002**, *124*, 3343-3353.

(23) Brydson, R. *Electron Energy Loss Spectroscopy*; BIOS Scientific: Oxford, 2001.

(24) Kresse, G.; Furthmuller, J. *Computational Materials Science* **1996**, *6*, 15-50.

(25) Kresse, G.; Furthmuller, J. *Physical Review B* **1996**, *54*, 11 169-186.

(26) Evans, H. T. *Nature Physical Science* **1971**, *232*, 69-70.

(27) Manna, L.; Scher, E. C.; Alivisatos, A. P. *Journal of the American Chemical Society* **2000**, *122*, 12700-12706.

(28) HRTEM images of binary nanorods indicate that the Cu_2S portions are in the high temperature phase of chalcocite. However, heating of the sample by the electron beam has previously been shown to convert Cu_2S films of low chalcocite into its high temperature phase (39)

(29) Cook, W. R. Jr; Shiozawa, L.; Augustine, F. *Journal of Applied Physics* **1970**, *41*, 3058-3063.

(30) Sands, T. D.; Washburn, J.; Gronsky, R. *physica status solida (a)* **1982**, *72*, 551-559.

(31) Wang, L.-W.; Li, J. *Physical Review B* **2004**, *69*, 153302 1-4.

(32) While the interface I_2 in Figure 5a connects the $(00\bar{1})$ Cu_2S facet to CdS, the interface I_2 in Figure 5c connects the (001) Cu_2S facet to CdS. However, given the similarities in bonding of Cu atoms to the interfacial sulfur layer in both interfaces, their formation energies should be similar.

(33) As the distortions occur primarily in the Cu_2S lattice, we define the angle of this interface by the angle between the CdS $(10\bar{1}2)$ and (0001) planes.

(34) The supercell shown in Figure 5e has been extended along the CdS [1000] direction and shortened

along the [10$\bar{1}$0] direction for clarity. The original supercell is shown in Supplementary Figure 4.

(35) Chan, E. M.; Marcus, M. A.; Fakra, S.; ElNaggar, M.; Mathies, R. A.; Alivisatos, A. P. *Journal of Physical Chemisty A* **2007**, *111*, 12210-12215.

(36) Manna, L.; Wang, L. W.; Cingolani, R.; Alivisatos, A. P. *Journal of Physical Chemisty B* **2005**, *109*, 6183-6192.

(37) Peng, Z. A.; Peng, X. *Journal of the American Chemical Society* **2001**, *123*, 1389-1395.

(38) Peng, X.; Wickham, J.; Alivisatos, A. P. *Journal of the American Chemical Society* **1998**, *120*, 5343-5344.

(39) Putnis, A. *American Mineralogist* **1977**, *62*, 107-114.